Contemporary Mathematics

A Lagged Diffusivity Method for Computing Total Variation Regularized Fluid Flow

Ranil Basnayake, Aaron Luttman, and Erik Bollt

Abstract. There is a great deal of recent work using optical flow methods for analyzing the dynamics of fluids, and much attention has been paid to developing regularization schemes for variational approaches that are consistent with the physics of fluid flow. In this work we show that using total variation to regularize two different kinds of optical flow functionals leads to very good flow field reconstructions for the kinds of dynamical structures that appear in fluid flow. The first optical flow functional is the classical component-based conservation of intensity, and the second approach is to reconstruct the potential of the flow, rather than the flow components. In the two cases, total variation regularization corresponds to imposing different scientific priors on the solution, which we compute using a variation of the Lagged Diffusivity Fixed Point Iteration. Numerical details are presented, and the results are demonstrated on synthetic data and on a data-driven oceanic flow model.

1. Introduction

Optical flow is the term used to describe the computation of the apparent flow field between two images of a particular scene. The original approach, introduced by Horn and Schunck in [**7**], imposed the assumptions that the flow be smooth and that intensity is locally conserved. Given image data $I(x, y, t)$, where $x, y \in \Omega \subset \mathbb{R}^2$ and $t \in [0, T]$, the flow field between two adjacent time instances $\langle u, v \rangle$ was computed as a minimizer of

$$E(u, v) = \int_\Omega (I_t + I_x u + I_y v)^2 \, d\Omega + \alpha \int_\Omega u_x^2 + u_y^2 + v_x^2 + v_y^2 \, d\Omega, \tag{1.1}$$

where $\alpha > 0$ is a regularization parameter. This method has been extended in many directions, including the introduction of new data fidelities [**1**, **4**] and regularization terms [**12**, **14**], as well as on numerical methods to enhance the accuracy and convergence of the corresponding algorithms [**5**]. In the case of imaging fluid dynamics, the flow is generally not smooth, and the the turbulent structures are those of greatest interest.

1991 *Mathematics Subject Classification.* Primary 49N45, 49M99; Secondary 65P10, 65T45.

Key words and phrases. Optical flow, Fluid Dynamics, Dynamical Systems, Total variation regularization.

This research was supported by the United States Office of Naval Research under Grant #N00014-09-1-0647.

In [**8**, **9**], it was shown that, rather than reconstructing the components $\langle u, v\rangle$ of the flow, it is possible to reconstruct the potential or stream function associated with the flow instead, when the flow is the gradient of a potential or the symplectic gradient of a stream. For either case of reconstructing the components or the associated potential, in order to more accurately capture dynamical structures in the flow, the optical flow functional can be regularized with the total variations of the flow components or the total variation of the potential function. It is well known that regularizing via the total variation results in signals that are approximately piecewise constant. In the case of regularizing with the total variation of the flow components, a flow whose components are piecewise constant will be favored. This is especially appropriate for laminar flows or flows that are approximately parallel to the coordinate axes. In the case of regularizing with the total variation of the potential (stream) function, the potential (stream) will be piecewise constant. This is especially appropriate for sparse flows. In this work we show that TV regularization also leads to excellent reconstructions of other flow structures such as vortices, hyperbolic fixed points, and sources and sinks, in both the component-based and potential-based formulations.

In order to minimize the TV-regularized optical flow functional, we linearize the associated Euler-Lagrange equations by adapting the Lagged Diffusivity Fixed Point Iteration (LDFPI) from [**13**]. In Section 2, we present the TV optical flow formulation and the LDFPI method. This is followed in Section 3 by results for synthetic data representing the dynamical structures of greatest interest for fluid flows, as well as to data generated from a data-driven ocean model of sea surface temperature data off the coast of Oregon, U.S.A..

2. Total Variation Regularized Optical Flow and LDFPI

The data fidelity term in (1.1) imposes the local conservation of intensity, and the regularization term enforces the smoothness of the flow field. If the flow is the gradient of a potential (or the symplectic gradient of a stream) function ψ, then (1.1) can be written

$$E(\psi) = \int_\Omega \left(I_t + \nabla I \cdot \nabla\psi\right)^2 \, d\Omega + \alpha \int_\Omega \psi_{xx}^2 + 2\psi_{xy}^2 + \psi_{yy}^2 \, d\Omega,$$

where ∇I is the spatial gradient of I for fixed t. In the case of a stream flow, rather than using the gradient of ψ, we use the symplectic gradient, $\nabla_H \psi = \langle -\psi_y, \psi_x\rangle$.

Rather than assuming the flow is smooth, however, we may instead regularize the flow using the total variation of the flow components or the potential function, resulting in the alternative optical flow functionals

$$E(u,v) = \int_\Omega \left(I_t + I_x u + I_y v\right)^2 \, d\Omega + \alpha \int_\Omega \left(|\nabla u| + |\nabla v|\right) \, d\Omega, \tag{2.1}$$

$$E(\psi) = \int_\Omega \left(I_t + \nabla I \cdot \nabla\psi\right)^2 \, d\Omega + \alpha \int_\Omega |\nabla\psi| \, d\Omega. \tag{2.2}$$

The resulting Euler-Lagrange equations for (2.1) are

$$\begin{aligned} I_x(I_t + I_x u + I_y v) + \alpha\nabla \cdot \left(\frac{\nabla u}{|\nabla u|}\right) = 0 \\ I_y(I_t + I_x u + I_y v) + \alpha\nabla \cdot \left(\frac{\nabla v}{|\nabla v|}\right) = 0, \end{aligned} \tag{2.3}$$

and, setting $K = -\nabla I \cdot \nabla$, the Euler-Lagrange equation for (2.2) is

$$K^* (I_t - K\psi) + \alpha \nabla \cdot \left(\frac{\nabla \psi}{|\nabla \psi|} \right) = 0, \tag{2.4}$$

where K^* is the operator adjoint of K.

The most straightforward approach to solving the system in (2.3) or the equation (2.4) is to use an explicit-time finite-difference discretization, but the convergence is far too slow to be practical in applications. In order to speed up the convergence, we linearize and solve using the Lagged Diffusivity Fixed Point Iteration.

The optical flow functionals (2.1) and (2.2) are least-squares, total-variation functionals of the form

$$E(f) = \|K(f) - h\|^2_{L^2(\Omega)} + \alpha TV(f), \tag{2.5}$$

where $f = \psi$ or $f = \langle u, v \rangle$, $K(u, v) = -I_x u - I_y v$ or $K\psi = -\nabla I \cdot \nabla \psi$, $h = I_t$, and $TV(f)$ is the total variation of ψ or the sum of the total variations of u and v. We use the standard approximation to the total variation of f, given by

$$TV(f) = \int_\Omega |\nabla f| \, d\Omega \approx \int_\Omega \sqrt{f_x^2 + f_y^2 + \beta} \, d\Omega$$

for a fixed numerical regularization $\beta > 0$.

Firstly, suppose that we wish to solve the Euler-Lagrange equations in (2.3), assuming the optical functional in (2.1). The flow components u and v are written as column vectors, and we define the column vectors

$$P_u = \frac{1}{\sqrt{u_x^2 + u_y^2 + \beta}} \quad \text{and} \quad P_v = \frac{1}{\sqrt{v_x^2 + v_y^2 + \beta}}.$$

The gradient of the approximate TV is then

$$L_n = \begin{bmatrix} D_x^T P_u D_x + D_y^T P_u D_y & 0 \\ 0 & D_x^T P_v D_x + D_y^T P_v D_y \end{bmatrix};$$

the data fidelity operator K is

$$K = \begin{bmatrix} -I_x & 0 \\ 0 & -I_y \end{bmatrix};$$

and the LDFPI algorithm is given by the iteration

(1) Compute gradient direction: $g_n = K^T(K[u_n, v_n]^T - [h, h]^T) + \alpha L_n [u_n, v_n]^T$
(2) Approximate Hessian: $H_n = K^T K + \alpha L_n$
(3) Quasi-Newton Step: $H_n [w_n, y_n]^T = -g_n$
(4) Solution update: $[u_{n+1}, v_{n+1}] = [u_n, v_n] + [w_n, y_n]$,

On the other hand, if we wish to solve the Euler-Lagrange equation in (2.4), assuming the optical flow functional in (2.2), then

$$P = \frac{1}{\sqrt{\psi_x^2 + \psi_y^2 + \beta}}, \quad L = D_x^T P D_x + D_y^T P D_y, \quad \text{and} \quad K = -I_x D_x - I_y D_y.$$

In this case, the iteration follows the same procedure, with $g_n = K^T(K\psi_n - h) + \alpha L_n \psi_n$, $H_n = K^T K + \alpha L_n$, $H_n s_n = -g_n$, and $\psi_{n+1} = \psi_n + s_n$.

In either case, one must select an appropriate initial condition, $[u_0^T, v_0^T]$ or ψ_0, which, in the case of optical flow, is usually chosen as the null flow or null potential. In the Quasi-Newton step, we use an LU factorization and Gaussian elimination.

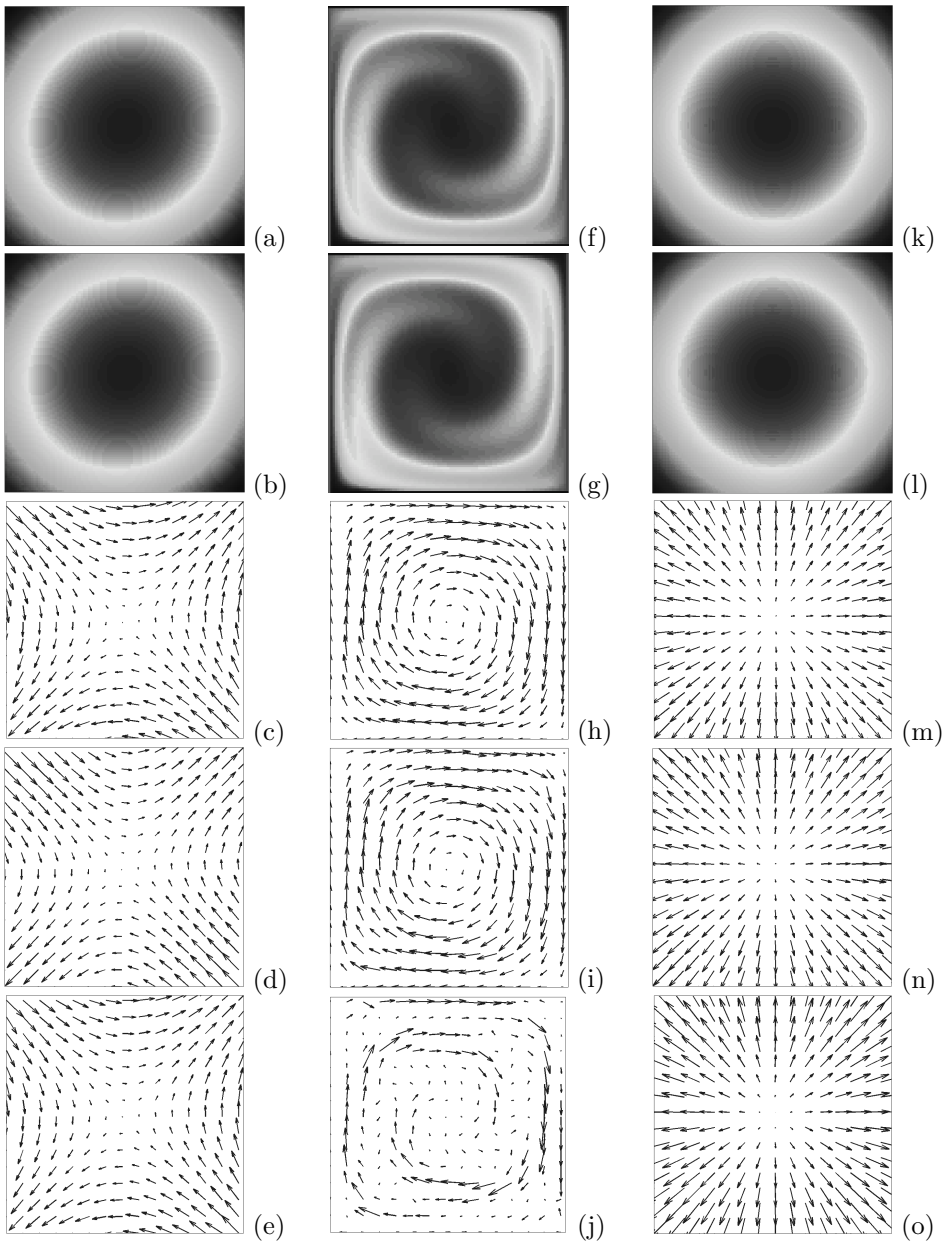

FIGURE 1. Flow Computations – Images (a),(b) show two time instances of the hyperbolic flow. Image (c) shows the true flow field between the images, and images (d),(e) present the computed flows for the u-v and ψ formulations, respectively. The second and third columns show the results for the gyre and diffusive flows.

For the results chosen here, the iteration is stopped when the relative change from one iteration to the next is sufficiently small.

3. Results of Optical Flow Calculations

In this section we present the results of our TV-regularized optical flow calculation on synthetic flows representing three different kinds of dynamical structures that are important in fluid dynamics, as well as results of the flow computation applied to data from a satellite data-driven ocean model.

For the first three synthetic sets, the data was obtained by choosing an initial density $I(x, y)$ and evolving it forward in time according to the continuity equation $\frac{dI}{dt} = -(I_x u + I_y v + I u_x + I v_y)$. The first example flow is about a hyperbolic fixed point, given by the velocity field $\langle u, v\rangle = \langle 2y, 2x\rangle$ on the domain $[-0.5, 0.5] \times [-0.5, 0.5]$. Two time instances of the density evolution can be seen in images (a) and (b) of Fig. 1. The true flow is shown in image (c), and the computed flows are shown in images (d) and (e), for the u-v and potential formulations, respectively. At least qualitatively, the images of the true and computed flows are quite similar. One method for measuring error in optical flow is the Mean Angular Error (MAE) [**10**], and in this case the resulting MAE is 2.24° for the u-v and 0.99° for the potential function total variation formulations. Both of these method outperform the Horn-Schunck method, which has an MAE of 5.31°.

The second data set is a so-called "gyre" flow about a vortex, given by the velocity field $\langle u, v\rangle = \langle -\pi \sin(\pi x)\cos(\pi y), \pi \cos(\pi x)\sin(\pi y)\rangle$ on $[0, 1] \times [0, 1]$. Note that this velocity is not the gradient of a potential function, but it is the symplectic gradient of a stream function, i.e.

$$\langle u, v\rangle = \langle -\psi_y, \psi_x\rangle$$

for $\psi(x, y) = \sin(\pi x)\sin(\pi y)$. Two time instances of the density evolution, the true flow, and the computed flows are shown in Fig. 1 (images (f)-(j)). In this case, the u-v formulation of total variation regularized flow is very close to the true flow– with an MAE of 2.58°–but the stream function formulation is not able to accurately reconstruct the gyre. This is due to the regularization, as a smoothness-based regularization is capable of reconstructing this flow within the stream function framework. In this case, the Horn-Schunck algorithm outperforms the TV-regularized u-v optical flow, but the two mean angular errors are quite close.

Two time instances of the flow about a source are shown in images (k) and (l) of Fig. 1, an evolution given by the velocity field $\langle u, v\rangle = \langle \cos x \cos y, -\sin x \sin y)\rangle$ on $[\frac{1}{4}\pi, \frac{3}{4}\pi] \times [\frac{3}{4}\pi, \frac{5}{4}\pi]$. The true flow is shown in image (m) and the computed flows in (n) and (o). The mean angular errors in this case are 1.674° and 1.45° for the u-v and potential TV optical flows, whereas the MAE for the Horn-Schunck method is 22.06°. In all three cases, the computed flows with TV in the u-v formulation capture the dynamical behaviors of the true flows, which is the fundamental goal when using an approach like this to analyze a fluid dynamical system.

For each of these computations, the regularization parameters α and β must be selected. There are numerous methods for choosing the regularization parameter α, such as the discrepancy principle, generalized cross-validation, or the L-curve method, but in these computations we have performed an exhaustive search to approximately choose α to minimize the mean angular error. The actual parameters chosen for the hyperbolic, gyre and diffusive data sets are $\alpha = 10^{-14}$, 10^{-14} and 3.16×10^{-8}, respectively, for the u-v formulation and $\alpha = 8.48 \times 10^{-14}$, 5.99×10^{-9} and 2.68×10^{-7}, respectively, for the potential/stream formulation. In each case, the minimum mean angular error corresponded to $\beta = 10^{-2}$.

TABLE 1. Mean Angular Errors for the Horn-Schunck method and the total-variation regularized, u-v and potential function formulations for hyperbolic, gyre, and diffusive synthetic flows.

Flow/Method	u-v TV	Potential TV	Horn-Schunck
Hyperbolic	2.24°	0.99°	5.31°
Gyre	2.58°	25.58°	2.26°
Diffusive	1.67°	1.45°	22.06°

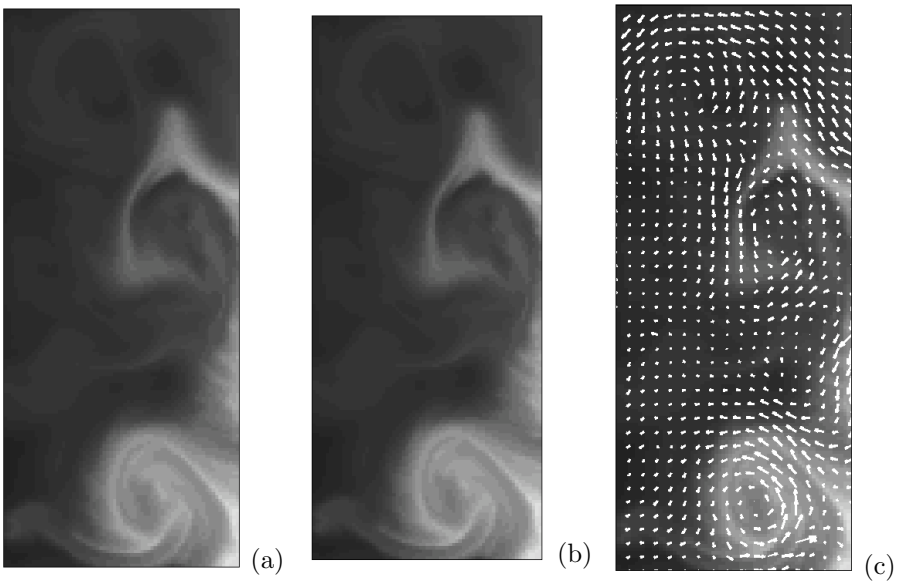

FIGURE 2. Sea Surface Temperature Flow Computations – Images (a) and (b) represent sea surface temperature off the coast of Oregon in August 2002. The lighter gray regions correspond to warmer surface temperatures and the darker regions to cooler temperatures. The computed flow with $\alpha = 10^{-5}$ is shown in (c).

3.1. Flow for oceanic data. Next we apply our method to compute the flow between time instances of the virtual flow of sea surface temperature off the coast of Oregon, U.S.A. This data set was generated from a 3-D ocean model using data obtained from the Geostationary Operational Environmental Satellite (GOES) as the initial condition. In Fig. 2 (a) and (b) represent two time adjacent images on August 1, 2002, representing sea surface temperature. In these images, light gray regions correspond to warmer surface temperatures, and the darker gray regions to cooler surface temperatures. It is clear that there are several vortices about which waters of like temperature are flowing but not mixing with the surrounding waters. These kinds of dynamical structures–and the resulting barriers and pseudo-barriers to transport–are important to study to understand the behavior of large-scale fluid dynamical systems, and the total variation, u-v formulation does a very good job

of capturing the vortices in the flow. The laminar flows in between the vortices are not captured as well, but it is the voriticial structures that are of the most interest when studying these dynamics.

4. Convergence Analysis of LDFPI for Optical Flow

The primary advantage to the LDFPI for optimizing total variation regularized problems is that the convergence of the scheme is very fast, especially when a good initial condition is chosen. As was noted above, for optical flow, the initial condition is usually chosen to be a null flow, and it turns out that this also results in very fast convergence of the algorithm, where numerical convergence is defined by thresholding the relative change in the solution from one iteration to the next.

Fig. 3 shows the mean angular error vs. iteration number for each of the three synthetic data sets analyzed above. The null flow results in an initial MAE of greater than 60°, and, in each case, the algorithm reduced that error in a very few iterations. Even though each iteration of the fixed point method is computationally more intensive than an iteration for an explicit-time scheme, in each case here–the TV-regularized u-v formulation for each of the 3 data sets and the TV-potential function formulation for the diffusive and hyperbolic data sets–the LDFPI method converges in fewer than 10 iterations.

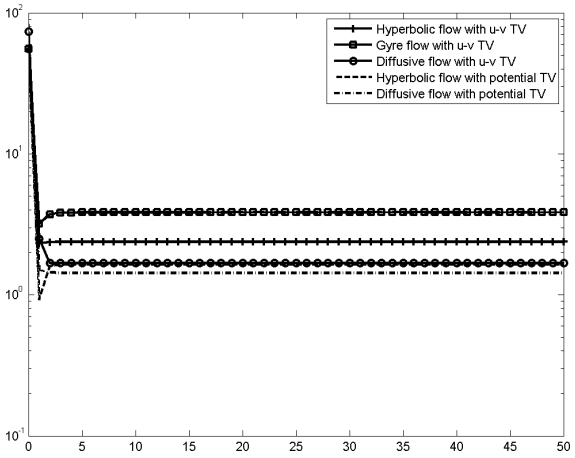

FIGURE 3. Mean Angular Error vs. Iteration Number – The computed mean angular error for the first 50 iterations with a fixed α for the hyperbolic, single gyre, and diffusive data sets.

5. Conclusions

In order to analyze the dynamics of fluid flows that are measured by imaging systems or are evolved as densities by ocean or other flow models, optical flow methods can be used to compute vector fields describing the flow. These vector fields can then be used to compute properties of the dynamics. In this work we have presented a total-variation regularized approach to optical flow in order to compute the components of the flow or to directly compute the potential function associated with the flow and have presented the lagged diffusivity fixed point iteration as a

highly efficient algorithm for computing the resulting flows. This approach gives accurate flow reconstruction results for the kinds of dynamics that are of interest in fluid flows, such as flows about hyperbolic and elliptic fixed points and flows out of a source.

Acknowledgements

The authors thank N. Tuffillaro for helpful comments and suggestions on the manuscript and working with the oceanic data and J. Osborne and A. Kurapov for providing access to data from their Regional Ocean Modeling System (ROMS) during the summer of 2002.

References

1. C. Brune, H. Maurer, and M. Wagner, "Detection of Intensity and Motion Edges within Optical Flow via Multidimensional Control," SIAM J. Imaging Science, **2** (2009), no. 4, 1190–1210.
2. T. Chang and P. Mulet, *On the convergence of the lagged diffusivity fixed point method in total variation image restoration*, SIAM J. Numer. Anal. **36** (1999), no. 2, 354–367. 1997.
3. P. Charbonnier, L. Blanc-fraud, G. Aubert and M. Barlaud, *Deterministic edge-preserving regularization in computed imaging*, IEEE Trans. Image Processing, **6** (1997), 298–311.
4. T. Corpetti, É. Mémin and P. Pérez, *Adaptation of Standard Optic Flow Methods to Fluid Motion*, 9th Int. Symp. Flow Visualisation, (2000), 1–10.
5. A. Doshi and A. G. Bors, "Navier-Stokes formulation for modeling turbulent optical flow," BMVC07, 2007, 10 pages.
6. D. Geman and C. Yang, *Nonlinear image recovery with half-quadratic regularization*, IEEE Trans. Image Processing **4** (1995), no. 7, 932–946.
7. B. K. P. Horn and B. G. Schunck, *Determining Optical Flow*, Artificial Intelligence **17** (1981), 185–203.
8. T. Kohlberger, É. Mémin, and C. Schnörr, "Variational dense motion estimation using the Helmholtz decomposition," in Scale Space '03, Vol. 2695, edited by L. D. Grin and M. Lillholm (2003), 432–448.
9. A. Luttman, E. Bollt, R. Basnayake, and S. Kramer, *A Stream Function Approach to Optical Flow with Applications to Fluid Transport Dynamics*, Proc. Appl. Math Mechanics, **11** (2011), no. 1, 855–856.
10. B. McCane, K. Novins, D. Crannitch, and B. Galvin, *On Benchmarking Optical Flow*, Computer Vision and Image Understanding **84** (2001), 126–143.
11. L. Rudin and S. Osher and E. Fatemi, *Nonlinear total-variation based noise removal algorithms*, Physica D: Nonlinear Phenomena **60** (1992), 259–268.
12. D. Suter, "Motion estimation and vector splines," in Proc. Conf. Comp. Vision Pattern Rec, 1994, 939–942.
13. C. R. Vogel, *Computational Methods for Inverse Problems*, SIAM, 2002.
14. J. Weickert, A. Bruhn, N. Papenberg and T. Brox, *Variational Optic Flow Computation: From Continuous Models to Algorithms*, International Workshop on Computer Vision and Image Analysis, 2003.

Department of Mathematics, Clarkson University, Potsdam, New York, 13699
E-mail address: basnayrk@clarkson.edu

National Security Technologies, LLC, P.O. Box 98521, M/S NLV078, Las Vegas, NV, 89193-8521
E-mail address: LuttmaAB@nv.doe.gov

Department of Mathematics, Clarkson University, Potsdam, New York, 13699
E-mail address: bolltem@clarkson.edu